Mass spectral characterization of submicron biogenic organic particles in the Amazon Basin

Q. Chen,[1] D. K. Farmer,[2] J. Schneider,[3] S. R. Zorn,[3] C. L. Heald,[4] T. G. Karl,[5] A. Guenther,[5] J. D. Allan,[6] N. Robinson,[6] H. Coe,[6] J. R. Kimmel,[2,7] T. Pauliquevis,[8] S. Borrmann,[3] U. Pöschl,[3] M. O. Andreae,[3] P. Artaxo,[8] J. L. Jimenez,[2] and S. T. Martin[1]

Received 8 July 2009; revised 8 September 2009; accepted 15 September 2009; published 28 October 2009.

[1] Submicron atmospheric particles in the Amazon Basin were characterized by a high-resolution aerosol mass spectrometer during the wet season of 2008. Patterns in the mass spectra closely resembled those of secondary-organic-aerosol (SOA) particles formed in environmental chambers from biogenic precursor gases. In contrast, mass spectral indicators of primary biological aerosol particles (PBAPs) were insignificant, suggesting that PBAPs contributed negligibly to the submicron fraction of particles during the period of study. For 40% of the measurement periods, the mass spectra indicate that in-Basin biogenic SOA production was the dominant source of the submicron mass fraction, contrasted to other periods (30%) during which out-of-Basin organic-carbon sources were significant on top of the baseline in-Basin processes. The in-Basin periods had an average organic-particle loading of 0.6 μg m^{-3} and an average elemental oxygen-to-carbon (O:C) ratio of 0.42, compared to 0.9 μg m^{-3} and 0.49, respectively, during periods of out-of-Basin influence. On the basis of the data, we conclude that most of the organic material composing submicron particles over the Basin derived from biogenic SOA production, a finding that is consistent with microscopy observations made in a concurrent study. This source was augmented during some periods by aged organic material delivered by long-range transport. **Citation:** Chen, Q., et al. (2009), Mass spectral characterization of submicron biogenic organic particles in the Amazon Basin, *Geophys. Res. Lett.*, *36*, L20806, doi:10.1029/2009GL039880.

1. Introduction

[2] Organic material (OM) typically constitutes 70 to 90% of the fine mass fraction in the Amazon Basin [*Fuzzi et al.*, 2007]. During the wet season, natural processes dominantly influence the loadings and the size distributions of the particles [*Andreae et al.*, 2002; *Martin et al.*, 2009]. These processes include the emission of PBAPs, the production of biogenic SOA, and the episodic input of marine and African particles by long-range transport. The fine-fraction organic-carbon (OC) loading is greater in the day than at night, perhaps because of enhanced SOA production by the photochemical oxidation of biogenic precursor gases [*Graham et al.*, 2003]. Speciation studies by chromatography show the presence in the fine fraction of methyltetrols, which are produced by the oxidation of isoprene [*Claeys et al.*, 2004]. Quantitative characterization of different OC sources in the Amazon Basin, however, is limited and challenging. The contribution of PBAPs such as bacteria and spores to the fine fraction is poorly understood and quantified [*Elbert et al.*, 2007]. The influence of downward convective mixing of particles from aloft (e.g., delivered by long-range transport) remains uncertain. These uncertainties result in loose constraints and hence limited accuracy for the modeling of scattering and absorption of solar radiation by submicron particles over the Amazon Basin and their activity as cloud condensation nuclei (CCN).

[3] In the wet season of 2008, as a part of the Amazonian Aerosol Characterization Experiment (AMAZE-08), we deployed a high-resolution time-of-flight aerosol mass spectrometer (AMS). This instrument conducts real-time measurements of the size-resolved chemical composition of non-refractory submicron particles [*DeCarlo et al.*, 2006]. Herein, we investigate the use of the mass spectra for characterizing the sources and properties of Amazonian particles.

2. Experiment

[4] Ground-based measurements were carried out from 7 Feb to 13 Mar 2008. The rain forest site (02° 35.68′S, 60° 12.56′W, 110 m above sea level), located 60 km NNW of Manaus, faced ca. 1600 km of nearly pristine forest to the east. The ten-day back trajectories indicated arrival of air masses from the northeast, originating over the Atlantic Ocean in the direction of Cape Verde and the Canary Islands. Aerosol from above the forest canopy (33 m) was sampled from the top of a tower ("TT34"; 38.75 m). The meteorological parameters at the tower top were 296/298 K (25 and 75% quantiles), 89/100% relative humidity (RH), and 995 ± 5 hPa during the measurement period. The aerosol was drawn to the ground in a turbulent flow of 40 to 80 L min^{-1} through a stainless steel tube (1.27 cm outside diameter), was passed through a Nafion dryer (exit

[1]School of Engineering and Applied Sciences and Department of Earth and Planetary Sciences, Harvard University, Cambridge, Massachusetts, USA.
[2]Department of Chemistry and Biochemistry and Cooperative Institute for Research in Environmental Science, University of Colorado, Boulder, Colorado, USA.
[3]Max Planck Institute for Chemistry, Mainz, Germany.
[4]Department of Atmospheric Science, Colorado State University, Fort Collins, Colorado, USA.
[5]National Center for Atmospheric Research, Boulder, Colorado, USA.
[6]National Centre for Atmospheric Science and School of Earth, Atmospheric and Environmental Sciences, University of Manchester, Manchester, UK.
[7]Aerodyne Research, Inc., Billerica, Massachusetts, USA.
[8]Applied Physics Department and Atmospheric Science Department, University of São Paulo, São Paulo, Brazil.

0094-8276/09/2009GL039880$05.00

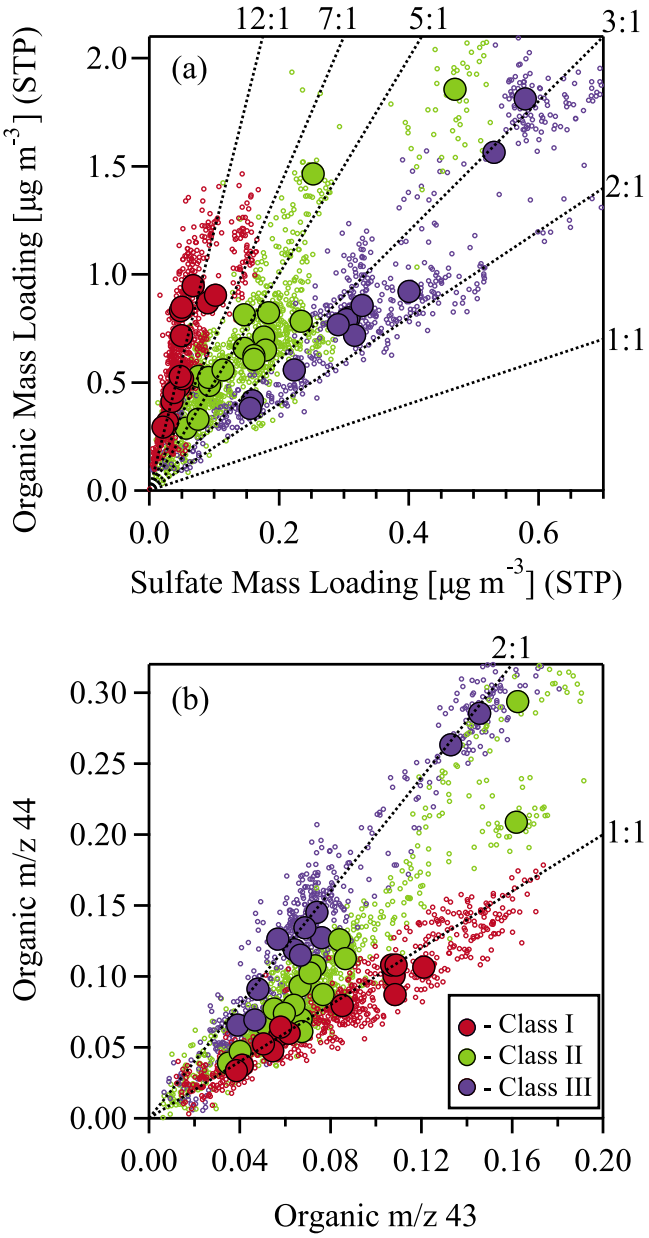

Figure 1. (a) Scatter plot of sulfate and organic mass loadings. (b) Scatter plot of signal intensities at *m/z* 43 and *m/z* 44 for the mass spectra of the organic material. For Figures 1a and 1b, large circles represent 12-h means of the shown 150-s data points. The classes I, II, and III are grouped by 12-h mean sulfate mass fractions of 0 to 0.12, 0.12 to 0.23, and above 0.23, respectively.

RH varied from 40% to 70%), and then was sampled by the AMS. Most of the results in this paper pertain to the data set collected using this AMS, but a second AMS operated by MPI-C sampled on a laminar-flow line (20 to 35% RH). The major results reported in this paper were confirmed by co-analysis of the MPI-C data set.

[5] The AMS data were processed by standard methods (see auxiliary material).[1] The mass loadings were adjusted to standard temperature and pressure (STP; 273 K and 10^5 Pa), which were approximately 10% greater than those at ambient conditions. A value of 1.0 was used for the AMS collection efficiency (a factor which potentially corrects for undetected particle mass) on the basis of the observation of liquid-like organic particles by microscopy [*Sinha et al.*, 2009]. With this collection efficiency, the campaign-average sulfate loading measured by the AMS (0.15 ± 0.03 μg m^{-3}; <1 μm) agreed within uncertainty with measurements made by ion chromatography (0.21 ± 0.06 μg m^{-3}; <2 μm) and particle-induced X-ray emission (0.24 ± 0.05 μg m^{-3}; <2 μm) for filter samples. For comparison, the average sulfate loading measured in four previous campaigns ranged from 0.17 to 0.26 μg m^{-3} in the wet season (cf. *Martin et al.*, 2009, Table 3). The campaign-average OM loading measured by the AMS was 0.7 ± 0.3 μg m^{-3} (<1 μm). This loading is at the low end of the range of 1.0 to 2.0 μg m^{-3} (<2.5 μm; OM:OC = 1.7) reported in the previous campaigns [*Fuzzi et al.*, 2007] (see auxiliary material for further explanation).

[6] For the analysis herein, 12-h mean daytime (06:00 to 18:00) and nighttime (18:00 to 06:00) mass loadings were calculated from the AMS data. Periods having low data coverage during a 12-h averaging time were removed. Measurement periods that were influenced by changes in local winds that could have caused the exhaust of the on-site power generator or regional anthropogenic outflow from Manaus to arrive at the tower were also excluded. Elemental oxygen-to-carbon (O:C) and hydrogen-to-carbon (H:C) ratios were calculated using 12-h high-resolution mass spectra [*Aiken et al.*, 2008].

3. Results and Discussion

[7] Correlative behavior between submicron organic and sulfate loadings, given the greater existing knowledge concerning the processes controlling sulfate and its precursors in the Amazon Basin, can give insight into the processes that influence the organic content. Sulfate is the predominant inorganic constituent of wet-season Amazonian particles [*Fuzzi et al.*, 2007]. Approximately 0.05 μg m^{-3} of the sulfate loading (<2 μm) has been attributed to in-Basin biogenic sources derived from sulfur-containing gases (e.g., DMS and H_2S) emitted from the rain forest ecosystem [*Andreae et al.*, 1990]. Sulfate loading above the ecosystem baseline occurs by out-of-Basin advective input of both marine-derived sulfate from the Atlantic Ocean and combustion-derived sulfate from Africa.

[8] During AMAZE-08, organic and sulfate loadings are well correlated within classes (Figure 1a). A histogram of sulfate mass fraction shows three modes (Figure S1), and consequently three classes I, II, and III of data points are colored in Figure 1 for low, moderate, and high sulfate mass fractions. The stratification by sulfate mass fraction further categorizes well the mass spectra of the organic material (Figure 1b). The ratio of the signal intensity at *m/z* 44 to that at *m/z* 43, which are the most intense in the organic mass spectra, is constant within uncertainty for each class. An elevated 44-to-43 ratio has been suggested as an indicator of more oxidized organic material [*Shilling et al.*, 2009]. As a group, the organic mass spectra within class I are self-similar and likewise within class III. Self-similarity is

[1] Auxiliary materials are available in the HTML. doi:10.1029/2009GL039880.

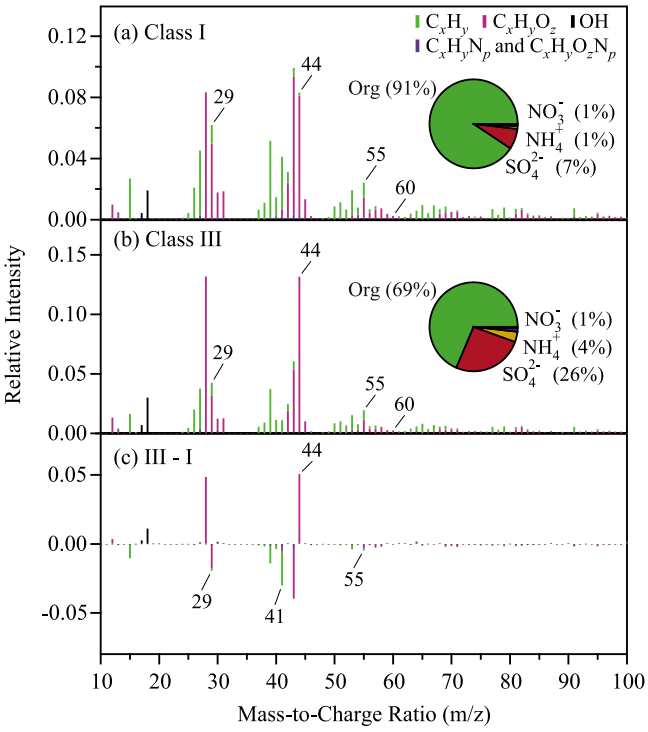

Figure 2. (a–b) Organic mass spectra representative of class I and III periods. Shown by coloring on the lines at each nominal *m/z* value are the relative contributions of the "C_xH_y", "$C_xH_yO_z$", "OH", "$C_xH_yN_p$", and "$C_xH_yO_zN_p$" families, as obtained by analysis of the high-resolution mass spectra. The shown mass-to-charge (*m/z*) ratios are truncated at 100, and the higher *m/z* values contribute no more than 5% to the total organic signal. Inset pie charts represent the period-average chemical composition. (c) A difference plot of the class I and class III spectra shown in Figures 2a and 2b.

defined by the criterion that the standard deviations of the relative intensities of prominent peaks are mostly within 15%, although there are a few exceptions (cf. Table S1). The spectra of class II can be divided into two sub-classes, one of which is similar to that of class I and the other to that of class III.

[9] These classifications can be associated with sources of the organic material. For instance, in-Basin biogenic SOA production can be concluded as the dominant source of submicron material during class I periods. The mass spectra (Figure 2a) have similar major peaks as those of laboratory SOA particles formed from the oxidation of individual biogenic precursors [*Bahreini et al.*, 2005; *Shilling et al.*, 2009]. High-resolution mass spectra of SOA particles, obtained in the Harvard Environmental Chamber (unpublished data) for the oxidation of isoprene, the monoterpene α-pinene, and the sesquiterpene β-caryophyllene, can be linearly combined to largely reproduce the patterns observed in AMAZE-08. The O:C ratio, which ranged from 0.39 to 0.45 (avg. 0.42; OM:OC $\approx$ 1.71) during class I periods, is also similar to that of laboratory SOA particles at realistically-low precursor concentrations (e.g., 0.40 to 0.45 by *Shilling et al.* [2009]). For comparison, urban-combustion primary emissions (O:C < 0.10) and aged regional particles (O:C $\approx$ 0.9) observed nearby Mexico City had significantly different values [*Aiken et al.*, 2008]. The conclusion is that, even though the molecular details are expected to have differences owing to the greater complexity of Amazonian production pathways (e.g., emissions and reactions) compared to laboratory processes, overall properties like the O:C ratio can still be similar. The explanation may be that volatility influences the partitioning between gas and particle phases and that a predictive factor of volatility can be the O:C ratio within many molecular classes.

[10] Some other plausible alternatives to an in-Basin SOA origin for class I particles, such as regional biomass burning, emissions of PBAPs, or an out-of-Basin influence, can be considered but ruled out. The mean sulfate loadings were below 0.1 μg m^3, a threshold value that is conservatively consistent with in-Basin sources (i.e., twice 0.05 μg m^{-3} taking into account uncertainty), thereby ruling out a significant out-of-Basin influence. The relative intensity of *m/z* 60, which is a fragment of levoglucosan and related species and serves as a marker of biomass burning, was less than 0.3% during AMAZE-08 and therefore indicating the absence of a significant influence of regional emissions from biomass burning [*Docherty et al.*, 2008]. In support, measurements using a PTR-MS during AMAZE-08 recorded benzene-to-acetonitrile ratios varying from 0.0 to 0.3, effectively setting a ten-day lower limit based on photochemical aging since the last exposure of an air mass to tropical biomass burning (i.e., a typical ratio of 1.0 at emission [*Karl et al.*, 2007]).

[11] Comparison of the mass spectra for model PBAPs (*J. Schneider*, unpublished data) to those for AMAZE-08 shows that characteristic peaks, such as *m/z* 60, 61, and 73 for carbohydrates like sugar alcohols and *m/z* 30, 42, and 56 for amino acids, constitute no more than 5% of the organic material during AMAZE-08. Furthermore, nitrogen-containing peaks expected for amino acids are negligibly present in the high-resolution mass spectra (cf. Figures 2a and 2b). Collaborators in AMAZE-08 imaged submicron particles collected on filters and observed that spherical organic particles that appear as liquid droplets are the main population [*Sinha et al.*, 2009], a result which is consistent with a dominant presence of biogenic SOA particles and a minor contribution of PBAPs to the submicron fraction.

[12] In contrast to class I periods, elevated mean sulfate loadings (i.e., 0.2 to 0.6 μg m^{-3}) suggest a significant contribution from out-of-Basin sources during class III periods. This contribution is further supported by the similarity of a representative organic mass spectrum (Figure 2b) to those of aged rural particles [*Zhang et al.*, 2005] and free-troposphere particles [*Hock et al.*, 2008]. A difference mass spectrum between class I and III highlights an elevated relative intensity at *m/z* 44 (Figure 2c), suggesting a contribution by highly oxidized materials [*Zhang et al.*, 2005]. The overall O:C ratio correspondingly increased during class III periods, with a range of 0.46 to 0.53 (avg. 0.49; OM:OC $\approx$ 1.79). Good candidates for the sources of these oxidized materials include emissions from African biomass burning [see *Capes et al.*, 2008, Figure 9d] and possibly the Atlantic Ocean, followed by in- and out-of-cloud photo- and oxidant processing during transport.

[13] Diel profiles shown in Figure 3 for AMAZE-08 are consistent with the above descriptions. The surface loadings

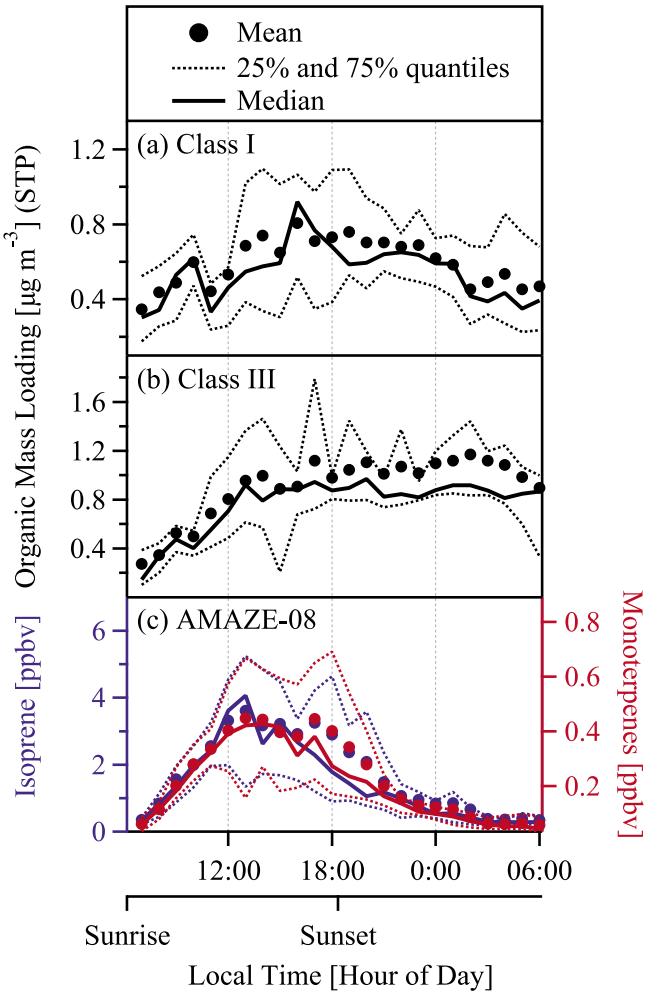

Figure 3. (a–b) Diel profiles of the organic loading during class I and III periods. (c) Diel profiles of the concentrations of isoprene and monoterpenes obtained using proton-transfer-reaction mass spectrometry (PTR-MS) [*Karl et al.*, 2009].

in the morning are influenced by the residual layer of the previous day (i.e., formed above the nocturnal boundary), day-to-day variability of boundary layer depth, and nighttime rainfall. For class I periods (Figure 3a), a doubling of the organic loading from the morning to the afternoon and a decline from the late afternoon to next morning are suggestive of photochemically initiated emissions and SOA production. The maximum (16:00; Figure 3a) is consistent with an earlier increase in the concentrations of isoprene and monoterpenes (13:00-15:00; Figure 3c), which are SOA precursor gases. The diel invariance of the *m/z* 44-to-43 ratio suggests a single source (Figure S2a), and its value (ca. 1.0) indicates little atmospheric aging. In comparison, for class III periods the *m/z* 44-to-43 ratio increases from approximately 1.3 to 2.0 in the morning and then maintains a steady state (Figure S2b), supporting the explanation of daytime convective downward mixing of aged organic particles from aloft. Consistent with this explanation, the organic loading increases more in the morning during class III than class I periods and then maintains an apparent steady state for the rest of the day (Figure 3b). The sulfate loading shows a similar but even stronger diel trend, providing further indication to the importance of long-range transport during class III periods (Figure S2d).

[14] In contrast to the clear stratifications of mean sulfate loadings of <0.1 and >0.1 μg m^{-3} during class I and III periods, respectively, the sulfate loading ranges from 0.06 to 0.47 μg m^{-3} during class II periods. The organic mass spectra are also better represented by two bifurcating branches, one closer to the spectra of class I and the other to that of class III, rather than as an average. The O:C ratios range from 0.37 to 0.55. Class II periods can therefore be explained as mixed periods during which the out-of-Basin influence is significant yet not fully emergent. For the period of study, we classify 40% of the time as dominantly affected by in-Basin sources, 30% as strongly influenced by out-of-Basin sources on top of the baseline in-Basin sources, and the remainder as having a significant but weaker out-of-Basin influence.

[15] The measurements reported herein can be put into greater context by comparison with the predictions of a chemical transport model. GEOS-Chem was employed (see auxiliary material) to simulate the loadings at the site during the time period of AMAZE-08. The simulated average organic loading was 35% lower than the measurement. This underprediction is several-fold smaller than simulation-measurement comparisons made for anthropogenically influenced regions [e.g., *Volkamer et al.*, 2006]. Although the reduction in the underprediction for the natural conditions of AMAZE-08 is encouraging as a metric for confidence in the accuracy and completeness of the underlying physics and chemistry of the simulation, the possibility of fortuitous cancelling of errors must be considered [*Capes et al.*, 2009]. Many uncertainties remain in the simulation, including the identification and emission rates of biogenic SOA precursors, the formation mechanisms (e.g., heterogeneous and aqueous processes), the accuracy of the included oxidant radical cycle to the Amazonian boundary layer [*Lelieveld et al.*, 2008], and the SOA particle mass yields [*Shilling et al.*, 2009].

[16] In summary, this paper presents the first real-time mass spectrometric measurements of the chemical composition of submicron Amazonian particles. The particles were largely composed of sulfate and organic material, having a campaign-average organic mass fraction of 0.78. The results further show that biogenic SOA production can dominate the submicron organic loading during times of diminished out-of-Basin influence. SOA production is expected to occur both in the gas and particle phases and in cloud waters, and this production is expected to strongly influence the size distribution and the chemical composition of submicron particles in the Amazon Basin, in turn regulating the CCN and optical properties of the particle population. During time periods of strong out-of-Basin influence, the organic loading increased on average from 0.6 to 0.9 μg m^{-3} (i.e., +50%). The material was also more oxidized, and this altered composition might be hypothesized to influence the physical or reactive properties of the particles.

[17] **Acknowledgments.** Support was received from the U.S. National Science Foundation, the German Max Planck Society, and Brazilian CNPq and FAPESP agencies. QC acknowledges a NASA Earth and Space Science Fellowship. DKF acknowledges a NOAA Global Change Fellowship.

References

Aiken, A. C., et al. (2008), O/C and OM/OC ratios of primary, secondary, and ambient organic aerosols with high-resolution time-of-flight aerosol mass spectrometry, *Environ. Sci. Technol.*, *42*, 4478–4485, doi:10.1021/es703009q.

Andreae, M. O., H. Berresheim, H. Bingemer, D. J. Jacob, B. L. Lewis, S.-M. Li, and R. W. Talbot (1990), The atmospheric sulfur cycle over the Amazon Basin: 2. Wet season, *J. Geophys. Res.*, *95*, 16,813–16,824, doi:10.1029/JD095iD10p16813.

Andreae, M. O., et al. (2002), Biogeochemical cycling of carbon, water, energy, trace gases, and aerosols in Amazonia: The LBA-EUSTACH experiments, *J. Geophys. Res.*, *107*(D20), 8066, doi:10.1029/2001JD000524.

Bahreini, R., et al. (2005), Measurements of secondary organic aerosol from oxidation of cycloalkenes, terpenes, and m-xylene using an aerodyne aerosol mass spectrometer, *Environ. Sci. Technol.*, *39*, 5674–5688, doi:10.1021/es048061a.

Capes, G., B. Johnson, G. McFiggans, P. I. Williams, J. Haywood, and H. Coe (2008), Aging of biomass burning aerosols over West Africa: Aircraft measurements of chemical composition, microphysical properties, and emission ratios, *J. Geophys. Res.*, *113*, D00C15, doi:10.1029/2008JD009845.

Capes, G., et al. (2009), Secondary organic aerosol from biogenic VOCs over West Africa during AMMA, *Atmos. Chem. Phys.*, *9*, 3841–3850.

Claeys, M., et al. (2004), Formation of secondary organic aerosols through photooxidation of isoprene, *Science*, *303*, 1173–1176, doi:10.1126/science.1092805.

DeCarlo, P. F., et al. (2006), Field-deployable, high-resolution, time-of-flight aerosol mass spectrometer, *Anal. Chem.*, *78*, 8281–8289, doi:10.1021/ac061249n.

Docherty, K. S., et al. (2008), Apportionment of primary and secondary organic aerosols in southern California during the 2005 Study of Organic Aerosols in Riverside (SOAR-1), *Environ. Sci. Technol.*, *42*, 7655–7662, doi:10.1021/es8008166.

Elbert, W., et al. (2007), Contribution of fungi to primary biogenic aerosols in the atmosphere: Wet and dry discharged spores, carbohydrates, and inorganic ions, *Atmos. Chem. Phys.*, *7*, 4569–4588.

Fuzzi, S., et al. (2007), Overview of the inorganic and organic composition of size-segregated aerosol in Rondonia, Brazil, from the biomass-burning period to the onset of the wet season, *J. Geophys. Res.*, *112*, D01201, doi:10.1029/2005JD006741.

Graham, B., et al. (2003), Composition and diurnal variability of the natural Amazonian aerosol, *J. Geophys. Res.*, *108*(D24), 4765, doi:10.1029/2003JD004049.

Hock, N., et al. (2008), Rural continental aerosol properties and processes observed during the Hohenpeissenberg Aerosol Characterization Experiment (HAZE2002), *Atmos. Chem. Phys.*, *8*, 603–623.

Karl, T. G., et al. (2007), The Tropical Forest and Fire Emissions Experiment: Method evaluation of volatile organic compound emissions measured by PTR-MS, FTIR, and GC from tropical biomass burning, *Atmos. Chem. Phys.*, *7*, 5883–5897.

Karl, T. G., et al. (2009), Rapid formation of isoprene photo-oxidation products observed in Amazonia, *Atmos. Chem. Phys.*, in press.

Lelieveld, J., et al. (2008), Atmospheric oxidation capacity sustained by a tropical forest, *Nature*, *452*, 737–740, doi:10.1038/nature06870.

Martin, S. T., et al. (2009), Sources and properties of Amazonian aerosol particles, *Rev. Geophys.*, doi:10.1029/2008RG000280, in press.

Shilling, J. E., et al. (2009), Loading-dependent elemental composition of alpha-pinene SOA particles, *Atmos. Chem. Phys.*, *9*, 771–782.

Sinha, B. W., et al. (2009), Composition and mixing state of wet season fine mode aerosol collected in the Amazonian tropical rain forest (Manaus, Brazil), *Geophys. Res. Abstr.*, *11*, Abstract EGU2009-4814.

Volkamer, R., J. L. Jimenez, F. San Martini, K. Dzepina, Q. Zhang, D. Salcedo, L. T. Molina, D. R. Worsnop, and M. J. Molina (2006), Secondary organic aerosol formation from anthropogenic air pollution: Rapid and higher than expected, *Geophys. Res. Lett.*, *33*, L17811, doi:10.1029/2006GL026899.

Zhang, Q., et al. (2005), Deconvolution and quantification of hydrocarbon-like and oxygenated organic aerosols based on aerosol mass spectrometry, *Environ. Sci. Technol.*, *39*, 4938–4952, doi:10.1021/es048568l.

J. D. Allan, H. Coe, and N. Robinson, National Centre for Atmospheric Science, University of Manchester, Manchester M60 1QD, UK.

M. O. Andreae, S. Borrmann, U. Pöschl, J. Schneider, and S. R. Zorn, Max Planck Institute for Chemistry, D-55128 Mainz, Germany.

P. Artaxo and T. Pauliquevis, Applied Physics Department, University of São Paulo, São Paulo CEP 05315-970, Brazil.

Q. Chen and S. T. Martin, School of Engineering and Applied Sciences, Harvard University, Cambridge, MA 02138, USA. (scot_martin@harvard.edu)

D. K. Farmer and J. L. Jimenez, Department of Chemistry and Biochemistry, University of Colorado, Boulder, CO 80309–0216, USA.

C. L. Heald, Department of Atmospheric Science, Colorado State University, Fort Collins, CO 80525–1371, USA.

A. Guenther and T. G. Karl, National Center for Atmospheric Research, P. O. Box 3000, Boulder, CO 80307–3000, USA.

J. R. Kimmel, Aerodyne Research, Inc., Billerica, MA, USA.

Supplementary Material

AMS Data Processing. AMS data were saved in 150-s intervals in alternating medium- and high-resolution modes [*DeCarlo et al.*, 2006]. The AMS data were processed using the software toolkit "Squirrel" with the "Pika" module,[1] including several updates to the fragmentation table [*Allan et al.*, 2004]. Specifically, the fragmentation coefficients at *m*/*z* 16, 17, 18, 29, 30, 39, 40, 44, and 46 were adjusted to account for the variability of gas-phase contributions and for the interference of ions having the same nominal *m*/*z*. Air contributions (e.g., $^{15}NN^+$ at *m*/*z* 29) were subtracted based on the data recorded with a HEPA filter in-line. Variations of the CO_2^+ signal at *m*/*z* 44 were corrected using measured gas-phase CO_2 concentration. The signals of CO^+ at *m*/*z* 28 and organic H_xO^+ at *m*/*z* 16, 17, and 18 were adjusted using the approach of *Aiken et al.*[2008]. The signals of NH_2^+ at *m*/*z* 16, NH_3^+ at *m*/*z* 17, NO^+ at *m*/*z* 30, NO_2^+ at *m*/*z* 46, and Ar^+ at *m*/*z* 40 were calculated as time-dependent fractions of the signals at unit resolution. $C_3H_3^+$ at *m*/*z* 39, which made up about 5% of the total organic signal, was calculated based on the ratio of $C_3H_3^+$ to Ar^+.

The campaign-average loading of organic material (OM) was 0.7 ± 0.3 μg m^{-3} (< 1 μm). This value is at the low end of the range of 1.0 to 2.0 μg m^{-3} reported in the previous campaigns (< 2.5 μm) [*Graham et al.*, 2003, and references therein; *Fuzzi et al.*, 2007]. In this comparison, a factor (OM:OC ≈ 1.7 [*Fuzzi et al.*, 2007]) is used by us for the conversion of OC reported in the previous studies to OM measured by the AMS. This OM:OC value is confirmed by the AMS result for AMAZE-08. Plausible explanations for the lower values reported herein include that approximately 30% of the fine-fraction OM measured in the previous studies was present in a size range of 1 to 2 μm, which lies

[1] http://cires.colorado.edu/jimenez-group/ToFAMSResources/ToFSoftware/.

outside the AMS measurement window, and that there were stronger influences from dust events and biomass burning in some of the previous studies not conducted in the middle of wet season and in other locations of the Amazon Basin.

Model Simulation. The GEOS-Chem global chemical transport model[2] was driven by GEOS-5 assimilated meteorology from the NASA Global Modeling and Assimilation Office. This model (v8.01.04) was employed here at a 2° × 2.5° horizontal resolution. Fossil fuel and biofuel emissions of organic carbon were as described by *Park et al.*[2003]. Daily biomass burning emissions were obtained by applying emission factors from *Andreae and Merlet* [2001] to estimate the daily burned area, as calculated from the Rapid Response MODIS product [*Justice et al.*, 2002; *Giglio et al.*, 2003] and the MODIS Vegetation Continuous Fields [*Hansen et al.*, 2003] for 2008, in an approach similar to that of *Wiedinmyer et al.*[2006]. We assumed that 50% of the emitted organic particles from combustion sources was hydrophobic, with an e-folding conversion of 1.2 days from hydrophobic to hydrophilic [*Cooke et al.*, 1999]. Organic particle mass loading resulting from secondary-organic-aerosol production from the oxidation of monoterpenes, isoprene, and other volatile organic compounds followed the two-product model of *Chung and Seinfeld* [2002] that is based on empirical fits to environmental chamber data. The simulated organic-carbon concentrations were scaled by a factor of two to account for additional non-carbon mass (i.e., OM:OC = 2) to obtain the simulated organic particle mass loadings. Coarse-mode PBAPs that can make a large contribution to PM_{10} mass loading were not included in the simulation and also are not measured by the AMS.

[2] http://www-as.harvard.edu/chemistry/trop/geos

Literature Cited

Aiken, A. C., et al. (2008), O/C and OM/OC ratios of primary, secondary, and ambient organic aerosols with high-resolution time-of-flight aerosol mass spectrometry, *Environ. Sci. Technol.*, *42*, 4478-4485.

Allan, J. D., et al. (2004), A generalised method for the extraction of chemically resolved mass spectra from aerodyne aerosol mass spectrometer data, *J. Aerosol Sci.*, *35*, 909-922.

Andreae, M. O., and P. Merlet (2001), Emission of trace gases and aerosols from biomass burning, *Global Biogeochem. Cycles*, *15*, 955-966.

Chung, S. H., and J. H. Seinfeld (2002), Global distribution and climate forcing of carbonaceous aerosols, *J. Geophys. Res., 107*(D19), doi:10.1029/2001JD001397.

Cooke, W. F., C. Liousse, H. Cachier, and J. Feichter (1999), Construction of a 1 degrees x 1 degrees fossil fuel emission data set for carbonaceous aerosol and implementation and radiative impact in the ECHAM4 model, *J. Geophys. Res., 104*, 22137-22162.

DeCarlo, P. F., et al. (2006), Field-deployable, high-resolution, time-of-flight aerosol mass spectrometer, *Anal. Chem.*, *78*, 8281-8289.

Fuzzi, S., et al. (2007), Overview of the inorganic and organic composition of size-segregated aerosol in Rondonia, Brazil, from the biomass-burning period to the onset of the wet season, *J. Geophys. Res., 112*, D01201, doi:01210.01029/02005JD006741.

Giglio, L., J. Descloitres, C. O. Justice, and Y. J. Kaufman (2003), An enhanced contextual fire detection algorithm for MODIS, *Remote Sens. Environ.*, *87*, 273-282.

Graham, B., et al. (2003), Composition and diurnal variability of the natural Amazonian aerosol, *J. Geophys. Res., 108*(D24), 4765, doi:4710.1029/2003JD004049.

Hansen, M., R. S. DeFries, J. R. G. Townshend, M. Carroll, C. Dimiceli, and R. A. Sohlberg (2003), Global Percent Tree Cover at a Spatial Resolution of 500 Meters: First Results of the MODIS Vegetation Continuous Fields Algorithm, *Earth Interact.*, *7*, 1-15.

Justice, C. O., et al. (2002), The MODIS fire products, *Remote Sens. Environ.*, *83*, 244-262.

Park, R. J., D. J. Jacob, M. Chin, and R. V. Martin (2003), Sources of carbonaceous aerosols over the United States and implications for natural visibility, *J. Geophys. Res., 108*(D12), doi:10.1029/2002JD003190.

Wiedinmyer, C., et al. (2006), Estimating emissions from fires in North America for air quality modeling, *Atmos. Environ.*, *40*, 3419-3432.

Table S1. Mean percent contributions of intense peaks to the total organic particle mass loadings in the 12-h averaged mass spectra. These peaks contribute more than 40% of the total organic loading for all classes. One standard deviation is shown in parentheses as a percentage of the mean contribution.

m/z	27	29	39	41	42	43	44	53	55	91
Ion Type	$C_2H_3^+$	$C_2H_5^+$ CHO^+	$C_3H_3^+$	$C_3H_5^+$	$C_2H_2O^+$	$C_2H_3O^+$	CO_2^+	$C_4H_5^+$	$C_4H_7^+$ $C_3H_3O^+$	$C_7H_7^+$
Class I	4.3 (3.2%)	5.4 (18%)	4.9 (5.2%)	3.9 (4.2%)	3.1 (3.2%)	9.6 (5.9%)	9.1 (4.9%)	1.8 (6.5%)	2.5 (4.6%)	0.8 (7.7%)
Class II	4.4 (8.6%)	3.7 (68%)	4.8 (10%)	3.0 (62%)	3.0 (8.1%)	8.4 (11%)	11 (8.5%)	1.9 (11%)	2.2 (6.5%)	0.6 (13%)
Class III	4.1 (9.6%)	3.6 (9.4%)	4.3 (15%)	2.6 (42%)	2.7 (12%)	6.9 (14%)	13 (6.2%)	1.8 (16%)	2.0 (6%)	0.5 (25%)

List of Figures

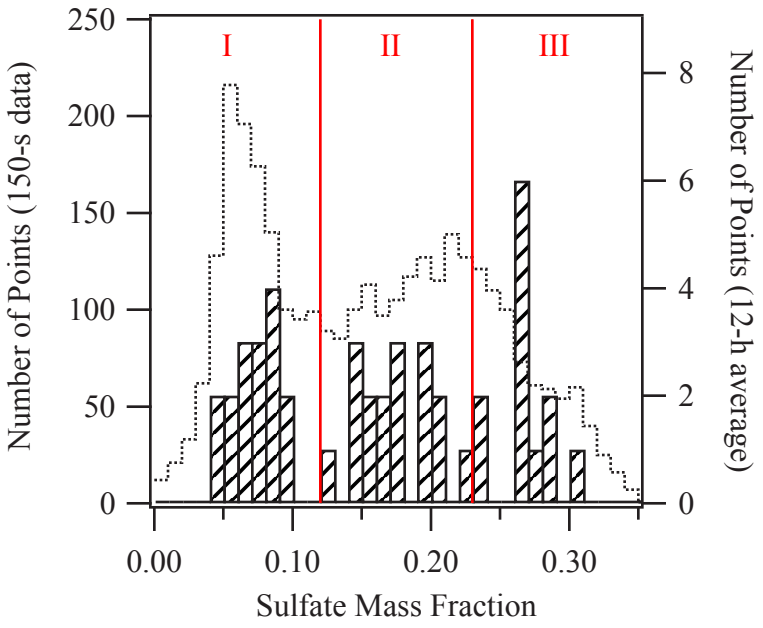
250
200
150
100
50
0
I
II
III
8
6
4
2
0
Number of Points (150-s data)
Number of Points (12-h average)
0.00
0.10
0.20
0.30
Sulfate Mass Fraction

Figure S1.

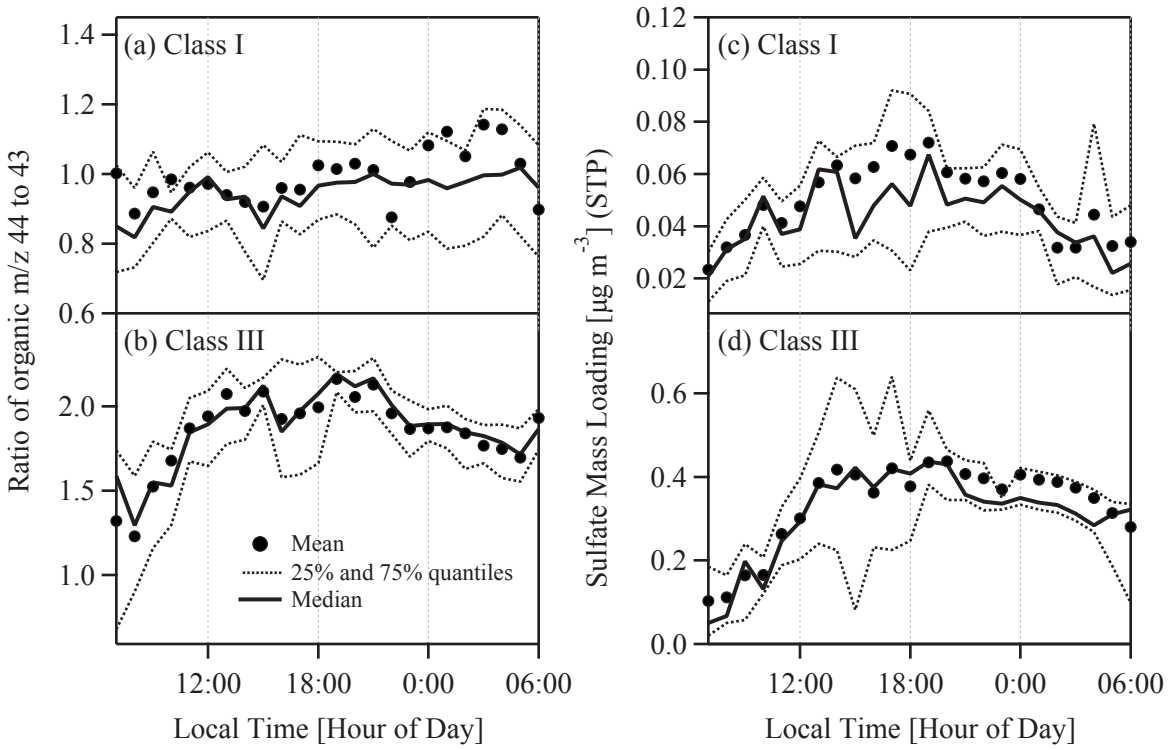
(a) Class I
(b) Class III
(c) Class I
(d) Class III
Ratio of organic m/z 44 to 43
Sulfate Mass Loading [μg m-3] (STP)
Mean
25% and 75% quantiles
Median
12:00
18:00
0:00
06:00
Local Time [Hour of Day]
Local Time [Hour of Day]

Figure S2.